Polypropylene/Wasted Poly(ethylene terephthalate) Fabric Composites Compatibilized by Two Different Methods: Crystallization and Melting Behavior, Crystallization Morphology, and Kinetics

Lin Zhidan, Shen Juncai, Chen Chao, Zhang Xiuju

College of Science and Engineering, Jinan University, Guangzhou 510632, People's Republic of China

Received 7 September 2010; accepted 14 November 2010
DOI 10.1002/app.33757
Published online 14 March 2011 in Wiley Online Library (wileyonlinelibrary.com).

ABSTRACT: Polypropylene (PP)/wasted poly(ethylene terephthalate) (PET) fabric composites and these composites modified by maleic anhydride grafted polypropylene (PP-*g*-MA) and reactive monomers were prepared with a twin-screw extruder. The crystallization morphology, nonisothermal crystallization and melting behavior, crystallization kinetics, and isothermal crystallization kinetics were investigated with differential scanning calorimetry. The results indicated that the wasted fabric (WF) had a heterogeneous nucleation effect on PP in the composites, and this increased the crystallization temperature and induced PP to form transcrystallinity. PP-*g*-MA further increased the crystallization temperature; however, the reactive monomers weakened the heterogeneous nucleation effect of WF. Also, the premelting temperature affected the crystallization and melting behavior of the composites significantly. The Avrami equation and the Mo method provided a fairly satisfactory description of the crystallization kinetics. The crystallization activation energy, nucleation constant, and folding surface free energy of PP were markedly reduced in the PP/waste PET fabric composites and the compatibilized composites. © 2011 Wiley Periodicals, Inc. J Appl Polym Sci 121: 1972–1981, 2011

Key words: compatibilization; composites; crystallization; differential scanning calorimetry (DSC); kinetics (polym.)

INTRODUCTION

Poly(ethylene terephthalate) (PET) is widely used in textile fiber products. However, nowadays, lots of PET textile fiber products are abandoned after short-term use in many countries because they are worn out, dirty, or out of fashion. It is a tremendous waste to bury or burn these wasted PET textile fiber products directly; their fabrication involved complicated processes and consumed large amounts of energy. From the viewpoint of global environmental protection and resource conservation, the recycling of these wastes is a great necessity and emergency. During past decades, numerous methods have been developed to recycle wasted PET products; these include the blending of recycled PET with virgin PET,[1,2] polyolefins,[3–12] and other polyesters,[13] the modification of PET with chain extenders,[14] incineration, and chemical recycling.[15] Among these methods, blending PET with polyolefins is very attractive because of the ease of fabrication, economy, and superior mechanical properties of the blends. Several articles have been published on blends of recycled PET and polyolefins.[3–12]

When PET fibers and polyolefins are blended at temperatures higher than their melting points, PET fibers lose their intrinsic fiber morphology and strength. In recent years, newly developed microfibrillar blends of polyolefins and polymers with a high melting point have exhibited specific properties comparable to those of polyolefin composites reinforced by mineral fibers,[16–19] and this is considered an effective reinforcement method for polyolefins. There have been many reports of binary microfibrillar blends of polyethylene and polyamide,[16] polyethylene and PET,[17] polypropylene (PP) and polyamide,[18] and PP and PET.[19] It is possible to both favorably enhance blends of polyolefins with wasted PET fabrics and maintain the fiber morphology of PET in the fabrics during melt blending. The key to attaining this goal is to solve the problem of dispersion from fabrics to filaments and the problem of interfacial adhesion between PET and polyolefins, which are incompatible with one another. According

Correspondence to: L. Zhidan (linzd@jnu.edu.cn).
Contract grant sponsor: Fundamental Research Funds for the Central Universities of China; contract grant number: 21609711.
Contract grant sponsor: Fundamental Research Foundation of Guangdong Province; contract grant number: 8451063201000041.

to our previous study,[20] when fabric flakes are too small, the shearing action during melt blending in a twin-screw extruder can disperse the flakes into the filaments. In this work, wasted PET fabric was used to reinforce a PP resin, and a macromolecular compatibilizer and reactive monomers were also used to improve the dispersion and interfacial adhesion of PP/wasted PET fabric composites. However, the ultimate mechanical properties of blends or composites based on crystallizable polymers are determined in part by the crystallization morphology, crystallization behavior, and crystallization kinetics. The main aim of this study was to investigate how wasted PET fabric and its interfacial modifiers affect the crystallization morphology, nonisothermal crystallization and melting behavior, nonisothermal crystallization kinetics, and isothermal crystallization kinetics of PP/wasted PET fabric composites.

EXPERIMENTAL

Materials

Commercial-grade isotactic PP (HP500N; melt flow rate = 12 g/10 min at 230°C) was supplied by Reliance Industries Limited, Hazira, India. Wasted PET fabric was obtained from recycled clothing (100% terylene) at a Chinese salvage station; the monofilament diameter was 20 μm. Maleic anhydride grafted polypropylene (PP-*g*-MA) was supplied by Guangzhou Lushan Chemical Materials Co. (Guangzhou, China) with an MA grafting ratio of 1.0% and a melt flow index of 15 g/10 min. Analytical-reagent-grade methyl methacrylate (MMA), styrene (St), and azodiisobutyronitrile were purchased from Tianjin Chemical Co., Ltd. (Tianjin, China).

Sample preparation

MMA, St, and azodiisobutyronitrile were mixed in a beaker in the ratio of 1:1:0.01. The wasted PET fabric was immersed in the monomer mixture for 1 h and then was squeezed until only 5 wt % of the mixture remained in the fabric. Subsequently, the fabric was heated at 80°C in an oven for 2 h to obtain the hardened fabric. Finally, the fabric was cut into 8 mm × 8 mm pieces and was named modified wasted fabric (MWF). Pure wasted fabric (WF) was also cut into 8 mm × 8 mm pieces.

PP, PP-*g*-MA, WF, and MWF were dried at 70°C for 24 h and were mixed according to the compositions listed in Table I. The mixtures were blended in a twin-screw extruder at 200°C. The extruded products were cooled at room temperature and crushed into small blocks in a breaker.

TABLE I
Compositions of the PP/Wasted PET Fabric Composites

	Component (wt %)			
Sample	PP	PP-*g*-MA	WF	MWF
PP	100	—	—	—
WF	—	—	100	—
F2	98	—	2	—
F5	95	—	5	—
F10	90	—	10	—
F15	85	—	15	—
G5F2	93	5	2	—
G5F5	90	5	5	—
G5F10	85	5	10	—
G5F15	80	5	15	—
MF2	98	—	—	2
MF5	95	—	—	5
MF10	90	—	—	10
MF15	85	—	—	15

Crystallization morphology

The crystallization morphology was studied with a polarizing microscope with a hot-stage thermal controller. The samples were placed between two cover glasses, melted at 230°C for 5 min, cooled to 125°C quickly, and then held there for 1 h.

Differential scanning calorimetry (DSC) characterization

A Q200 differential scanning calorimeter (TA Instruments Ltd, Crawley, West Sussex, United Kingdom) was used to study the thermal behavior of the PP/PET fabric composites and was calibrated with the melting temperature and enthalpy of a pure indium standard. An 8–9-mg sample was accurately weighed for DSC testing, and all measurements were performed in a nitrogen atmosphere.

For nonisothermal crystallization and melting behavior characterization, a composite sample was rapidly heated to 220°C (or 290°C) and held there for 5 min. Subsequently, it was cooled to 60°C at the cooling rate of 20°C/min for the crystallization behavior study. Then, it was reheated to 220°C (or 290°C) at 20°C/min for the melting behavior study.

For the study of the nonisothermal crystallization kinetics, a composite sample was rapidly heated to 220°C and held there for 5 min. Subsequently, it was cooled to 60°C at selected cooling rates ranging from 5 to 40°C/min. Each sample was used only once.

For the study of the isothermal crystallization kinetics, a composite sample was rapidly heated to 220°C and held there for 5 min. Subsequently, it was cooled to the crystallization temperature at the cooling rate of 100°C/min. The isothermal temperatures ranged from 126 to 130°C in steps of 1°C, and the

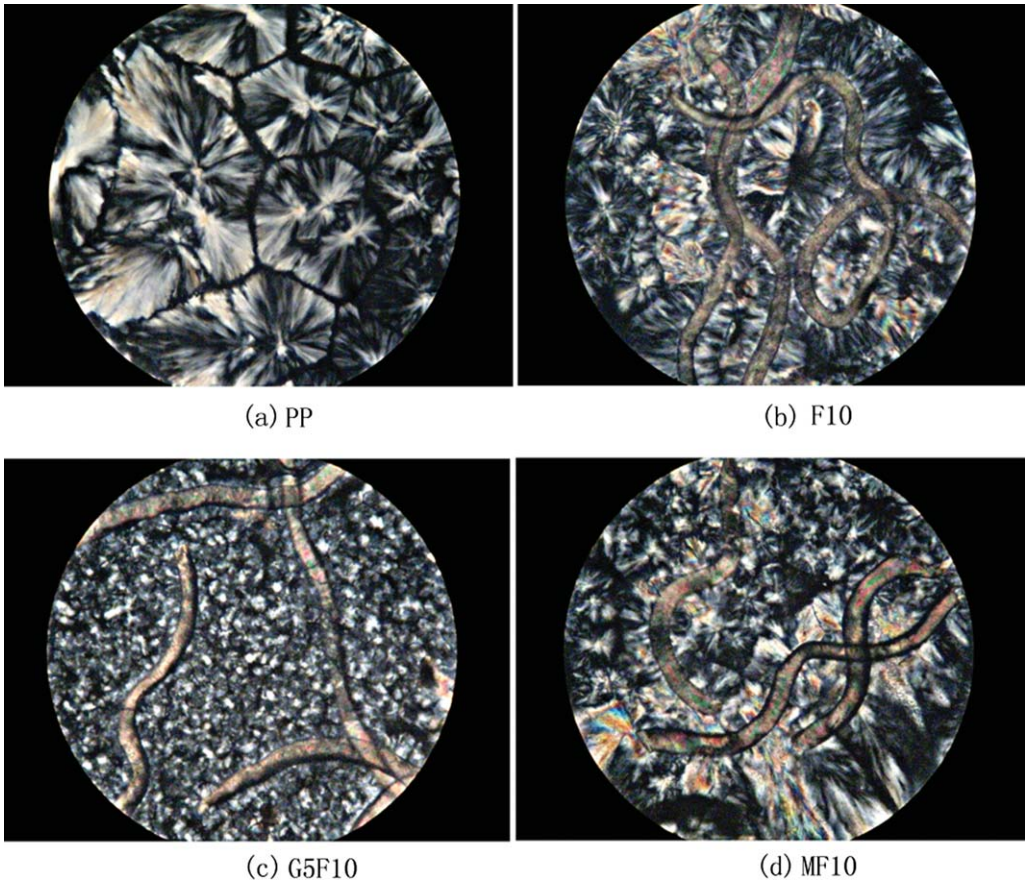

Figure 1 POM micrographs of the PP/WF composite, the PP-*g*-MA-modified PP/WF composite, and the MMA/St-modified PP/WF composite with 10 wt % WF. [Color figure can be viewed in the online issue, which is available at wileyonlinelibrary.com.]

sample was held at each isothermal temperature for 25 min to obtain complete crystallization. To observe the melting behavior, we reheated the isothermally crystallized samples to 220°C at the rate of 20°C/min.

RESULTS AND DISCUSSION

Crystallization morphology

The final performance of crystalline polymer matrix composites depends on the crystallization behavior and crystallization morphology of the polymer matrix to a large degree. In this study, the crystallization morphology of pure PP, an unmodified PP/WF composite, a PP-*g*-MA-modified PP/WF composite, and an MMA/St-modified PP/WF composite with 10 wt % WF was observed with polarized optical microscopy (POM; see Fig. 1). Spherulites with a black cross extinction phenomenon and an obvious crystal interface were observed in pure PP [Fig. 1(a)]. In the unmodified F10 composite [Fig. 1(b)], WF fiber with a diameter of 20 μm could be clearly observed. The transcrystallinity formed perpendicularly to the fiber surface in the region near the fiber surface, and this could explain why the melting temperature increased in comparison with that of pure PP. However, normal spherulites still formed in the region away from the fiber surface. Trivial crystals were seen in the PP-*g*-MA-modified G5F10 composite both near and far from the fiber surface. This might have been due to the fact that PP-*g*-MA, which exhibited a heterogeneous nucleation effect, was dispersed uniformly in the PP matrix. When the crystallization temperature was reached, lots of nuclei, which retarded the growth of the crystal, formed in an instant. A condition similar to that of the F10 composite was observed for the MMA/St-modified MF30 composite; the arrangement of transcrystallinity perpendicular to the fiber surface was less regular than that of the F10 composite. This may have been due to the fact that the copolymer of MMA and St disturbed the growth of transcrystallinity.

Nonisothermal crystallization and melting behavior

Figure 2 illustrates the DSC crystallization and melting curves of PP and wasted PET fabric. Meanwhile, the corresponding data are listed in Table II. The

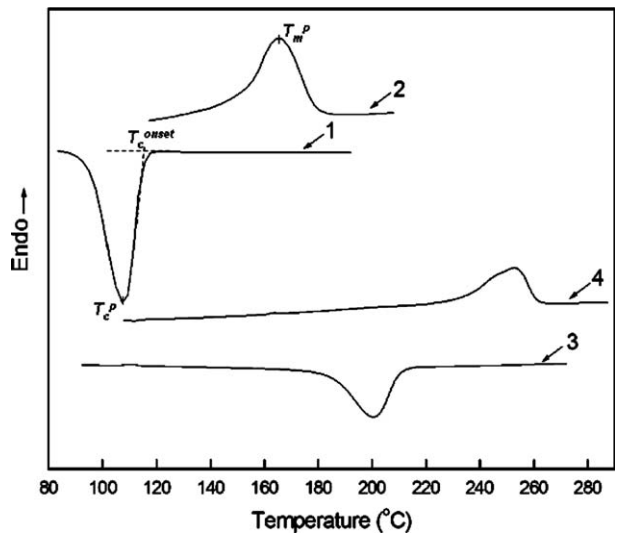

Figure 2 DSC crystallization and melting thermographs of (1,2) pure PP and (3,4) wasted PET fabric.

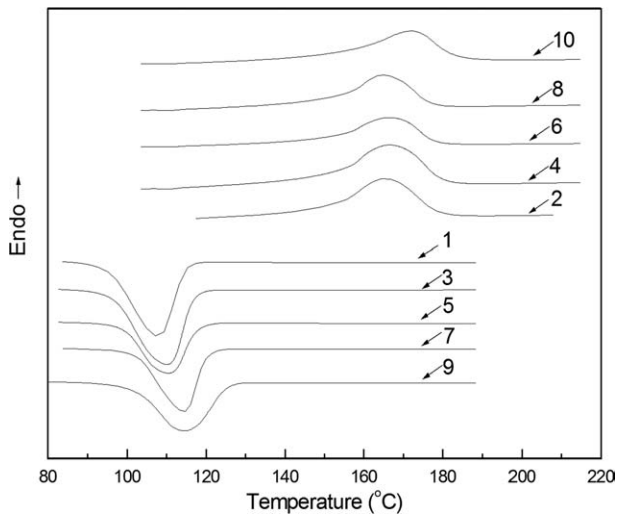

Figure 3 DSC crystallization and melting thermographs of (1,2) PP and (3,4) F2, (5,6) F5, (7,8) F10, and (9,10) F15 composites

peak melting temperatures (T_m^p, see figure 2) value of PP and wasted PET fabric were 163.60°C and 253.08°C, respectively, and they exhibited great differences. Therefore, it could be concluded that the wasted PET fabric did not melt and retained its original fiber morphology at the blending temperature of 200°C in this study.

Figure 3 shows the DSC crystallization and melting curves of pure PP and PP/WF composites, and the corresponding data are listed in Table II. The crystallization enthalpy (ΔH_c) and the melting enthalpy (ΔH_m) were normalized by the weight percentage of PP. The peak crystallization temperature (T_c^p) and onset crystallization temperature (T_c^{onset}) of PP were increased when it was blended with WF. Moreover, T_c^p of the composites increased with increasing WF content. This indicates that WF had a heterogeneous nucleation effect on PP crystallization and enabled PP crystallization at a higher temperature. Tao and Mai[21] and Li et al.[19] reported similar results when they were investigating PP/PET blends. T_c^p of the composite with 10 wt % WF (F10) was close to that of the composite with 15 wt % WF (F15), and this indicates that 10 wt % WF was saturated and had a heterogeneous nucleation effect on PP crystallization. Both ΔH_c and ΔH_m of the PP/WF composites were smaller than those of pure PP. The aforementioned POM results showed that irregular spherulites with a lower crystallization degree formed in the region away from the fiber surface, although compact transcrystallinity with a higher crystallization degree formed near the WF fiber. The effect of the latter overrode that of the former, and this reduced ΔH_c and ΔH_m of PP in the PP/WF composites. When it was blended with WF, PP in the PP/WF composites exhibited higher T_m^p values than pure PP, and this indicates that WF might induce the formation of transcrystallinity.

TABLE II
Nonisothermal Crystallization and Melting Parameters of Pure PP and PP/WF, PP-*g*-MA-Modified PP/WF, and PP/MWF Composites

Sample	T_c^p (°C)	T_c^{onset} (°C)	ΔH_c (J/g)	T_m^p (°C)	ΔH_m (J/g)
PP	107.14	115.02	98.13	163.60	95.64
WF	200.40	210.21	39.08	253.08	38.98
F2	109.98	116.65	90.41	166.40	84.02
F5	110.43	117.60	87.32	166.34	83.64
F10	114.08	121.05	97.38	165.14	94.06
F15	114.44	121.64	90.22	171.95	83.52
G5F2	109.25	116.88	90.71	166.15	84.53
G5F5	113.15	120.46	94.44	168.81	87.23
G5F10	114.51	121.84	92.59	168.26	86.78
G5F15	114.29	122.60	91.66	170.10	83.73
MF2	112.00	117.33	92.34	166.49	87.35
MF5	113.59	118.32	95.41	166.62	90.19
MF10	113.31	119.32	92.87	166.53	85.62
MF15	113.51	118.97	97.34	167.73	88.05

Figure 4 presents the DSC crystallization and melting curves of pure PP and PP/WF composites modified by PP-*g*-MA (the G5F*xx* series composites), and the related data can be seen in Table II. The PP/WF composites modified by PP-*g*-MA exhibited higher T_c^p values than pure PP. In comparison with the PP/WF composites, the G5F2 and G5F15 composites possessed T_c^p values close to those of the F2 and F15 composites, respectively, whereas the G5F5 and G5F10 composites exhibited T_c^p values higher than those of the F5 and F10 composites, respectively. The crystallization process of PP involves three-dimensional spherulite growth controlled by heterogeneous nucleation, and it was reported that the addition of PP-*g*-MA reduced the interfacial free

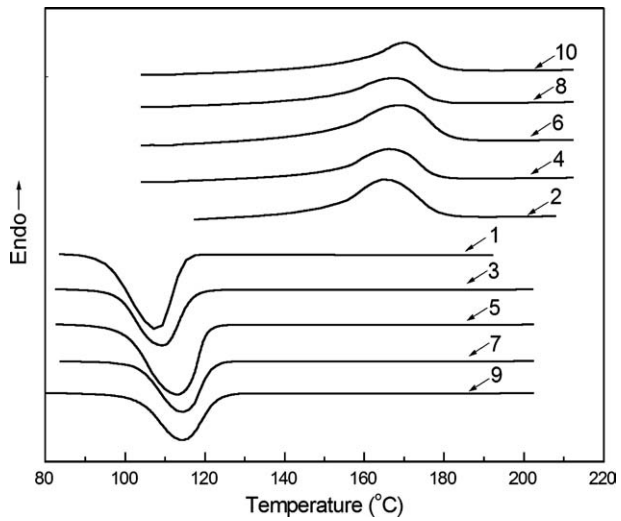

Figure 4 DSC crystallization and melting thermographs of (1,2) PP and (3,4) G5F2, (5,6) G5F5, (7,8) G5F10, and (9,10) G5F15 composites.

energy of the surfaces of crystal nuclei and promoted heterogeneous nucleation of PP.[22] In this study, T_c^p of the composites containing WF and PP-*g*-MA was higher than that of the composites containing only WF. This indicates that PP-*g*-MA also had a heterogeneous nucleation effect on PP crystallization, and this agrees with the reports of Wang et al.[23] and Seo et al.[24] Similarly, the PP/WF composites modified by PP-*g*-MA exhibited obviously higher T_m^p values than pure PP because of the formation of transcrystallinity

The DSC crystallization and melting curves of pure PP and PP/WF composites modified by reactive monomers (the MF*xx* series composites) are shown in Figure 5, and the related data are listed in Table II. During blending with MWF, T_c^p of PP in the composites increased to more than 112.00°C. However, a further increase in the MWF content did not markedly affect T_c^p of PP in the composites when the MWF content was greater than 5 wt %. In comparison with the F*xx* series and G5F*xx* series composites, the MF*xx* composites possessed higher T_c^p values than the F*xx* and G5F*xx* composites when the fabric content was less than 5 wt %. Meanwhile, the situation was reversed when the fabric content was more than 5 wt %. Hence, the modification of monomers weakened the heterogeneous nucleation effect of wasted PET fabric on PP crystallization. From the viewpoint of promoting the crystallization of PP, the threshold value for MWF is 5 wt %. According to the values of T_m^p, there also may be transcrystallinity in PP/WF composites modified by monomers.

Figure 6 shows the DSC crystallization and melting curves of F15, G5F15, and MF15 composites that were premelted at 220 and 290°C, respectively, to eliminate their heat history. After the heat history was eliminated at 290°C, the crystallization peak shapes of all the studied composites became markedly sharper in comparison with the shapes after the elimination of the heat history at 220°C. T_c^p of PP in the F15 and MF15 composites changed little, but T_c^p of PP in the G5F15 composite was obviously improved. It was concluded that WF melted and became dispersed in PP after the heat history was eliminated at 290°C. The dotted line in Figure 6 also shows the melting and crystallization of WF. In the G5F15 composite, without disturbing the fabric fibers, PP-*g*-MA more obviously exhibited a heterogeneous nucleation effect on PP in the composite and led to a marked increase in T_c^p. In the MF15

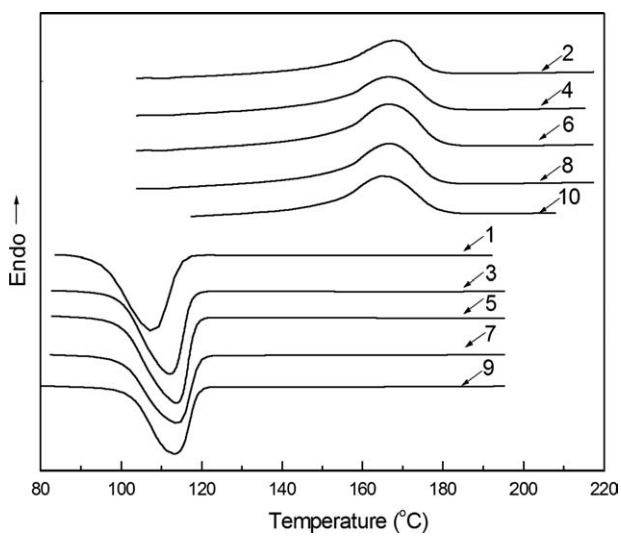

Figure 5 DSC crystallization and melting thermographs of (1,2) PP and (3,4) MF2, (5,6) MF5, (7,8) MF10, and (9,10) MF15 composites.

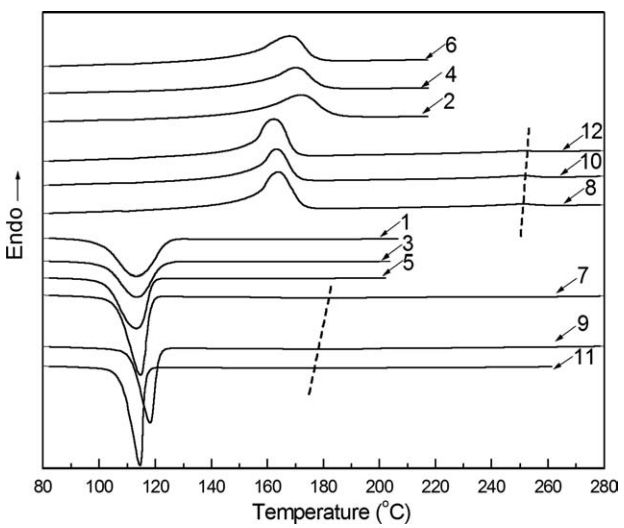

Figure 6 DSC crystallization and melting thermographs of (1,2,7,8) F15, (3,4,9,10) G5F15, and (5,6,11,12) MF15 composites premelted at 220 and 290°C.

composite, the resultant reactive monomers covering the WF surface entered the dispersed PET phase and did not affect the crystallization behavior of PP much. After the heat history at 290°C was eliminated, T_m^p of PP in all the studied composites decreased to 163°C, which was close to T_m^p of pure PP and at which normal PP spherulites formed. This demonstrated that the wasted PET fabric had an induction effect of transcrystallinity.

Nonisothermal crystallization kinetics

Four methods have been widely adopted to describe the nonisothermal crystallization process: the Avrami equation, the Ozawa equation, the Jeziorny equation, and the Mo method. The double-logarithmic form of the Avrami equation is as follows:[25]

$$\ln\{-\ln[1 - X(T)]\} = \ln Z_t + n\ln t \quad (1)$$

where $X(T)$ is the relative crystallinity after crystallization time t and Z_t and n are the crystallization kinetic constant and Avrami exponent, respectively (both are related to the rate and mechanism of crystallization).

Jeziorny[26] calibrated the crystallization kinetic constant of the Avrami equation with cooling rate Φ:

$$\log Z_c = \log Z_t/\Phi \quad (2)$$

where Z_c is the calibrated crystallization kinetic constant.

Ozawa[27] derived an equation; its double-logarithmic form is as follows:

$$\log\{-\ln[1 - X(T)]\} = \log K(T) - m\log R \quad (3)$$

where R is the cooling rate; $K(T)$ is a function related to the overall crystallization rate that indicates how fast the crystallization proceeds; and m is the Ozawa index, which is somewhat similar to n and depends on the type of nucleation and growth dimensions.

By combining the Avrami and Ozawa equations, Mo et al.[28] proposed a different equation that shows a relationship between cooling rate R and crystallization time t at a given relative crystallinity:

$$\log Z_t + n\log t = \log K(T) - m\log R \quad (4)$$

$$\log R = \log F(T) - \alpha\log t \quad (5)$$

where the kinetic parameter $F(T) = [K(T)/Z_t]^{1/m}$ refers to the value of the cooling rate, which has to be chosen at the unit of crystallization time when the measured system has a certain degree of crystallinity, and $\alpha = n/m$ is the Mo exponent. $F(T)$ has a definite physical and practical meaning: the smaller the value of $F(T)$ is, the higher the crystallization rate is.

Moreover, Kissinger[29] had suggested a method to determine the activation energy for the transport of the macromolecular segments to the growing surface, ΔE, by calculating the variation of T_c^p with the cooling rate Φ:

$$d\left[\ln\left(\Phi/T_c^{p2}\right)\right]/d\left(1/T_c^p\right) = -\Delta E/R \quad (6)$$

where R is the gas constant T_c^p is the peak crystallization temperature.

With eqs. (1)–(6), plots of the nonisothermal crystallization kinetics of the F10 composite [see Fig. 7(a–d)] were obtained, and they showed good linearity with the Avrami method, the Mo method, and the Kissinger method. This suggests that these three methods may provide a satisfactory description of the composites in this study. All the nonisothermal crystallization kinetic parameters of the composites with 10 wt % fabric are listed in Table III according to the same calculating procedures used for the F10 composite. For pure PP, approximately $2.8 < n < 3.4$ was observed, and this suggests spherulite growth from nuclei initiated at time zero; this agrees with the relevant literature.[30] The n values of the F10, G5F10, and MF10 composites also ranged from 2.8 to 3.4, and this means that the wasted PET fabric, PP-*g*-MA, and reactive monomers did not influence the nucleation form and crystal growth form of PP to a large extent. With the cooling rate increasing, the crystallization half-time ($t_{1/2}$) and T_p of the pure PP and the F10, G5F10, and MF10 composites decreased. At the same cooling rate, $t_{1/2}$ and T_p of the F10, G5F10, and MF10 composites were smaller than those of pure PP (especially for the G5F10 composite). $F(T)$ and α of the pure PP and the F10, G5F10, and MF10 composites increased with increasing $X(T)$, and this suggests that a more rapid cooling rate was needed to reach a certain value of $X(T)$ within the same crystallization time. With the same value of $X(T)$, the values of $F(T)$ for these specimens ranked as follows: PP > F10 > G5F10 > MF10. That is, to reach the same value of $X(T)$, the crystallization time needed by PP was longest, whereas the crystallization time of the MF10 composite was shortest. This demonstrated the heterogeneous nucleation effect of the fabric, reactive-monomer-modified fabric, and PP-*g*-PP. Moreover, the values of ΔE for these specimens ranked as follows: PP > MF10 > F10 > G5F10. This indicates that the addition of the wasted PET fabric obviously depressed ΔE of PP in the composites and made the crystallization of PP in the composites easier under nonisothermal crystallization conditions.

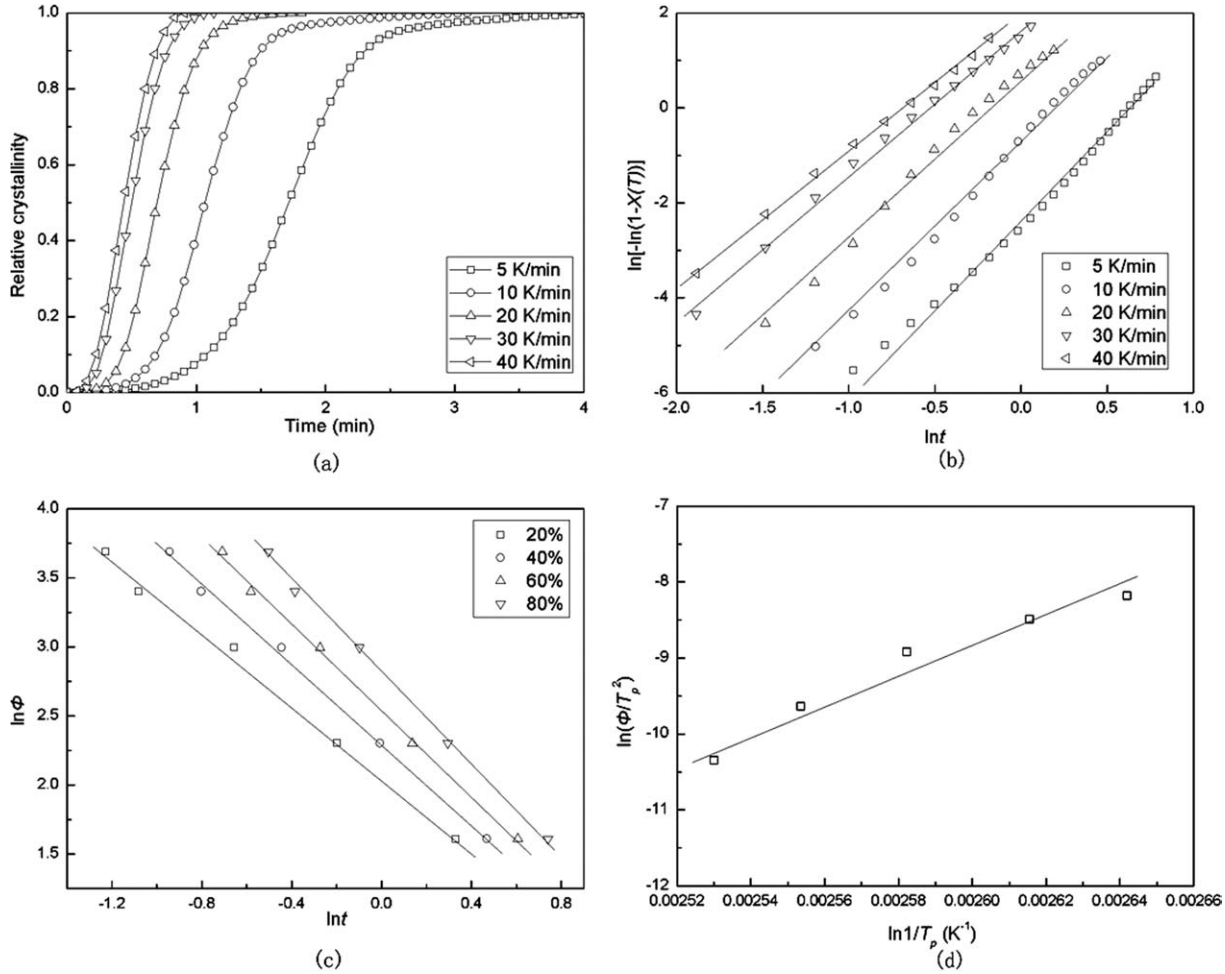

Figure 7 Nonisothermal crystallization kinetic plots of the F10 composite: (a) curves of the relative crystallinity versus time, (b) Avrami plots at various cooling rates, (c) Mo plots at various crystallinities, and (d) a Kissinger plot.

TABLE III
Nonisothermal Crystallization Kinetic Parameters of Pure PP and PP/WF, PP-*g*-MA-Modified PP/WF, and PP/MWF Composites with 10 wt % Fabric

Sample	Φ (°C/min)	n	Z_c	$t_{1/2}$ (min)	T_p (°C)	ΔE (kJ/mol)	X(T) (%)	F(T) (K min^{a-1})	α
PP	5	3.4	0.62	1.71	115.45	221.16	20	7.1	1.4
	10	3.1	0.95	0.96	111.72		40	9.3	1.4
	20	3.3	1.06	0.59	107.14		60	11.5	1.5
	30	2.8	1.07	0.48	105.44		80	14.4	1.6
	40	3.0	1.06	0.45	103.82				
F10	5	3.1	0.64	1.71	122.08	158.23	20	6.6	1.4
	10	3.2	0.90	0.91	118.43		40	9.0	1.5
	20	3.1	1.09	0.69	114.08		60	11.0	1.6
	30	3.1	1.06	0.49	109.16		80	14.3	1.6
	40	2.8	1.05	0.43	105.34				
G5F10	5	2.8	0.66	1.53	123.14	146.45	20	5.9	1.4
	10	3.2	0.91	0.95	119.81		40	8.3	1.5
	20	3.2	1.05	0.65	114.51		60	10.8	1.6
	30	3.1	1.04	0.47	109.32		80	14.2	1.7
	40	3.1	1.05	0.41	105.22				
MF10	5	3.4	0.68	1.40	121.46	165.58	20	5.1	1.7
	10	2.7	0.96	0.88	118.55		40	7.5	1.8
	20	2.9	1.06	0.61	113.31		60	10.3	1.9
	30	3.1	1.04	0.55	109.50		80	14.8	2.1
	40	2.9	1.05	0.46	105.59				

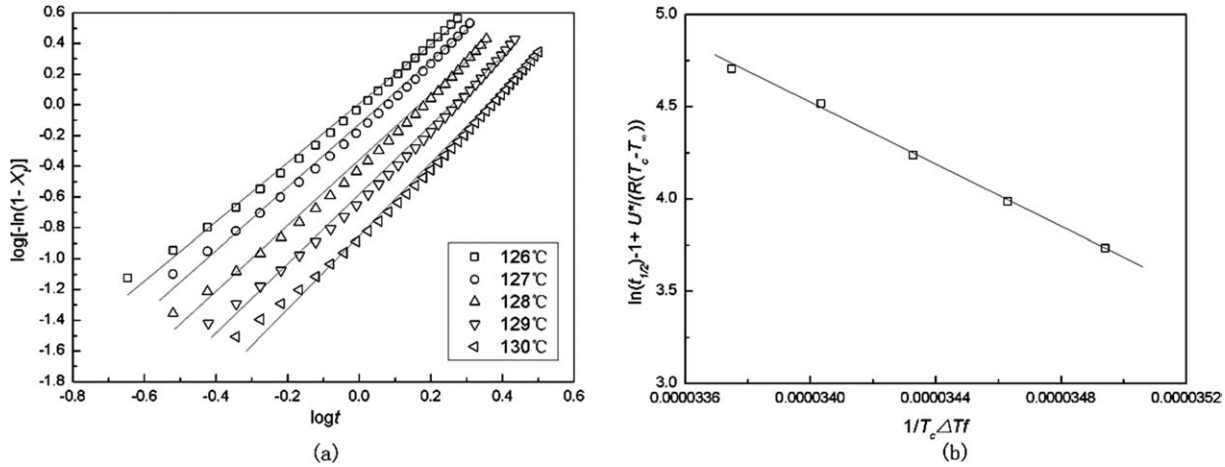

Figure 8 Isothermal crystallization kinetic plots of the F10 composite: (a) Avrami plots at different temperatures and (b) a plot according to the Lauritzen–Hoffman equation.

Isothermal crystallization kinetics

The Avrami equation is widely used to describe isothermal crystallization processes in polymers:

$$1 - X_t = \exp(-Kt^n) \tag{7}$$

where X_t is the volume crystallinity at time t; K is the overall kinetic rate constant; and n is the Avrami exponent, which depends on the nucleation and growth mechanism of the crystal.

In general, the Avrami equation[31] is often converted into the traditional linear form:

$$\log[-\ln(1 - X_t)] = \log K + n\log t \tag{8}$$

In our experiment, so-called Avrami plots of $\log[-\ln(1-X_t)]$ versus $\log t$ were computed to obtain the values of K and n.

According to Hoffman's model,[32] the spherulite growth rate (G) can be written as follows:

$$G = G_0\exp[-U*/R(T_c - T_\infty)]\exp\left[-K_g/T_c\Delta Tf\right] \tag{9}$$

where G_0 is is a preexponential factor generally assumed to be constant, K_g is the nucleation constant, T_∞ is the hypothetical temperature at which all motion associated with viscous flow ceases (233.5 K for PP), T_c is the crystallization temperature, $\Delta T = T_m{}^0 - T_c$ (where $T_m{}^0$ is the equilibrium melting temperature) is the undercooling (481 K for PP), f is the factor expressed by $2T_c/(T_m{}^0 - T_c)$ that accounts for the change in the heat of function as the temperature is reduced below $T_m{}^0$, R is the gas constant (8.314 J K mol), and U^* is the activation energy for the transportation of segments to the crystallization site (6270 J/mol for PP). G can be taken as $1/t_{1/2}$, and the logarithmic form of Hoffman's equation can be written as follows:

$$\ln\left(t_{1/2}\right)^{-1} + U^*/R(T_c - T_\infty) = A - K_g/T_c\Delta Tf \tag{10}$$

where A is in G_0.

The free energy of folding can be obtained as follows:

$$K_g = 4\ \sigma\sigma_e b_0 T_m{}^0/k\ \Delta H \tag{11}$$

$$\sigma = ab_0\ \Delta H \tag{12}$$

where b_0 is the layer thickness (6.56×10^{-10} m for PP), σ is the lateral surface free energy (9.2×10^{-3} J/m^2 for PP), σ_e is the folding surface free energy, ΔH is the enthalpy of fusion (1.4×10^8 J/m^3 for PP), and k is the Boltzmann constant (1.38×10^{-23} J/K).

In our experiment, a plot of $\ln(t_{1/2})^{-1}+U^*/R(T_c - T_\infty)$ versus $1/T_c\Delta Tf$ was computed to obtain the values of K_g and σ_e. This plot provided K_g as a slope.

According to eqs. (7)–(12), plots of the isothermal crystallization kinetics of the F10 composite [see Fig. 8(a,b)] were obtained, and they showed good linearity with the Avrami method and the Hoffman method; this suggests that these two methods may provide a satisfactory description of the composites in this study. The parameters of all specimens are listed in Table IV. Pure PP had a value of approximately $2.1 < n < 2.3$, and this suggests a two-dimensional, circular, diffusion-controlled growth of nucleation in this temperature range.[30] The n values of the F10, G5F10, and MF10 composites also ranged from 2.0 to 2.4, and this means that the wasted PET fabric, PP-*g*-MA, and reactive monomers did not influence the nucleation form and crystal growth form of PP under the isothermal crystallization conditions. With an increase in the isothermal crystallization temperature, K decreased

TABLE IV
Isothermal Crystallization Kinetic Parameters of Pure PP and PP/WF, PP-*g*-MA-Modified PP/WF, and PP/MWF Composites with 10 wt % Fabric

Sample	T_c (°C)	n	K (min^{-n})	$t_{1/2}$ (min)	$G_{1/2}$ (min^{-1})	K_g (10^6 K^{-2})	σ_e (J/m^2)
PP	130	2.1	0.016	6.02	0.166	0.94	0.159
	129	2.1	0.030	4.59	0.218		
	128	2.3	0.035	3.66	0.273		
	127	2.2	0.065	2.81	0.356		
	126	2.2	0.120	2.17	0.461		
F10	130	2.3	0.129	2.04	0.490	0.83	0.138
	129	2.3	0.230	1.63	0.613		
	128	2.3	0.385	1.30	0.769		
	127	2.1	0.686	1.01	0.990		
	126	2.1	0.953	0.86	1.163		
G5F10	130	2.2	0.319	1.44	0.694	0.53	0.088
	129	2.2	0.502	1.16	0.862		
	128	2.0	0.835	0.91	1.099		
	127	2.2	0.895	0.89	1.124		
	126	2.2	0.988	0.86	1.163		
MF10	130	2.1	0.040	3.42	0.292	0.91	0.151
	129	2.4	0.064	2.69	0.372		
	128	2.3	0.146	2.07	0.483		
	127	2.2	0.284	1.6	0.625		
	126	2.2	0.466	1.29	0.775		

and $t_{1/2}$ increased in all specimens. This was due to the fact that at a high crystallization temperature, the thermal motion of the macromolecular segments became intense, and this was against the formation of nuclei and the growth of crystals. At the same crystallization temperature, the K values ranked as follows: G5F10 > F10 > MF10 > PP. This indicates that the fabric, the fabric modified by reactive monomers, and PP-*g*-MA were favorable to the formation of nuclei and the growth of crystals, accelerated the crystallization rate of PP, and reduced $t_{1/2}$. The heterogeneous nucleation effect of the PP matrix composites under the isothermal crystallization conditions could be embodied by K_g and σ_e. The K_g values of all specimens ranked as follows: PP > MF10 > F10 > G5F10. The σ_e values ranked in the same order. The smaller the K_g and σ_e values were, the easier the formation of nuclei in the polymer melts was. PP-*g*-MA remarkably reduced the crystallization σ_e value of PP in the G5F10 composite and was beneficial to the isothermal crystallization of PP. This result agrees with the results for nonisothermal crystallization kinetics reported in a previous section.

CONCLUSIONS

Wasted PET fabric had a heterogeneous nucleation effect on PP: it increased the crystallization temperature and induced the transcrystallinity of PP in the PP/wasted PET fabric composites. Compatibilization methods influenced the crystallization and melting behavior of the compatibilized PP/wasted PET fabric composites. PP-*g*-MA further increased the crystallization temperature, but the reactive monomers weakened the heterogeneous nucleation effect of the wasted PET fabric. The premelting temperature also affected the crystallization and melting behavior of the composites. The Avrami equation, the Mo method, and the Hoffman method provided a fairly satisfactory description of the crystallization kinetics. The activation energy, nucleation constant, and folding surface free energy of PP were remarkably reduced in the PP/wasted PET fabric composites and the compatibilized composites. From the viewpoint of promoting the crystallization of PP, the G5F10 composite exhibited a better modification effect in comparison with the other composites.

References

1. Oromiehie, A.; Mamizadeh, A. Polym Int 2004, 53, 728.
2. Awaja, F.; Pavel, D. Eur Polym J 2005, 41, 2614.
3. Fakirov, S.; Kamo, H.; Evstatiev, M.; Friedrich, K. J Macromol Sci Phys 2004, 43, 775.
4. Avila, A. F.; Duarte, M. V. Polym Degrad Stab 2003, 80, 373.
5. Morawiec, J.; Krasnikova, N. P.; Galeski, A.; Pracella, M. J Appl Polym Sci 2002, 86, 1486.
6. Pawlak, A.; Morawiec, J.; Pazzagli, F.; Pracella, M.; Galeski, A. J Appl Polym Sci 2002, 86, 1473.
7. Evstatiev, M.; Fakirov, S.; Krasteva, B.; Friedrich, K.; Covas, J. A.; Cunha, A. M. Polym Eng Sci 2002, 42, 826.
8. Pawlak, A.; Morawiec, J.; Galeski, A. Polimery 2002, 47, 491.
9. Pluta, M.; Bartczak, Z.; Pawlak, A.; Galeski, A.; Pracella, M. J Appl Polym Sci 2001, 82, 1423.
10. Friedrich, K.; Evstatiev, M.; Fakirov, S.; Evstatiev, O.; Ishii, M.; Harrass, M. Compos Sci Technol 2005, 65, 107.
11. Oyman, Z. O.; Tincer, T. J Appl Polym Sci 2004, 89, 1039.
12. Akovali, G.; Karababa, E. J Appl Polym Sci 1998, 68, 765.
13. Fraisse, F.; Verney, V.; Commereuc, S.; Obadal, M. Polym Degrad Stab 2005, 90, 250.

14. Torres, N.; Robin, J. J.; Boutevin, B. J Appl Polym Sci 2001, 79, 1816.
15. Lorenzetti, C.; Manaresi, P.; Berti, C.; Barbiroli, G. J Polym Environ 2006, 14, 89.
16. Denchev, Z.; Oliveira, M. J.; Carneiro, O. S. J Macromol Sci Phys 2004, 1, 143.
17. Wan, H. Q.; Ji, X. J Mater Sci 2004, 39, 6839.
18. Zoldan, J.; Siegmann, A.; Narkis, M. J Macromol Sci Phys 2005, 44, 495.
19. Li, Z. M.; Yang, W.; Li, L. B.; Xie, B. H.; Huang, R.; Yang, M. B. J Polym Sci Part B: Polym Phys 2004, 42, 374.
20. Lin, Z.; Zhang, X.; Shen, J. J Polym Eng 2009, 29, 521.
21. Tao, Y.; Mai, K. Eur Polym J 2007, 43, 3538.
22. Zhang, J.; Xie, X.; Ke, H. Acta Polym Sinica 2002, 1, 13.
23. Wang, Y.; Shen, H.; Li, G.; Mai, K. J Therm Anal Calorim 2010, 99, 399.
24. Seo, Y.; Kim, J.; Kim, K. U.; Kim, Y. C. Polymer 2000, 41, 2639.
25. Avrami, M. J Chem Phys 1940, 8, 212.
26. Jeziorny, A. Polymer 1978, 19, 1142.
27. Ozawa, T. Polymer 1971, 12, 150.
28. Liu, T. X.; Mo, Z. S.; Wang, S. E.; Zhang, H. F. Polym Eng Sci 1997, 37, 568.
29. Kissinger, H. E. J Res Natl Bur Stand 1956, 57, 63.
30. Wu, D. F.; Wu, L.; Wu, L. F.; Xu, B.; Zhang, Y. S.; Zhang, M. J Polym Sci Part B: Polym Phys 2007, 45, 1100.
31. Avrami, M. J Chem Phys 1939, 7, 1103.
32. Hoffman, J. D. Polymer 1983, 24, 3.